INDIVIDUAL BLADE PITCH CONTROL OF FWT

Contents

4.1 Introduction

In the previous chapters, the controllers based on nonlinear approaches (SAST, ASTW,...) have been designed based on the collective blade control technology. Generally, these controllers have better performances in term of control objectives, *i.e.* power regulation and platform pitch reduction than the baseline GSPI. Moreover, structure loads have been also compared with those obtained by the baseline controller and the controllers provide satisfying results. Notice that the load reduction is not a specific control objective; it is checked after the control design in order to make sure that the controllers do not excite large structure loads. In fact, the structure loads are become more and more important with the increasing capacity and flexibility of wind turbines; such loads are harmful to the system, reduce the service life and increase the costs of maintenance (Petrović, Jelavić, and Baotić 2015; Menezes Novaes, Araújo, and Bouchonneau Da Silva 2018). Floating wind turbines,

especially need to withstand wind, waves and complex marine environments as well as the motions excited by the floating structure. All of those factors induce much larger structure loads than conventional onshore wind turbines (Jason Mark Jonkman 2007). Therefore, reducing the fatigue loads is a key-point (E. A. Bossanyi 2003; Menezes Novaes, Araújo, and Bouchonneau Da Silva 2018) for wind turbines. The control strategy must provide an efficient solution for such problems and appears crucial for floating wind turbine systems.

Therefore, besides regulating the power and reducing the platform pitch motion, the controller proposed in this chapter takes the load reduction into consideration. Among the structure loads, the load of blade root, being the source of the loads for the rest of the structures, is one of the most important (Jelavić, Petrović, and Perić 2010). Hence, it is specifically considered as a control objective by introducing an additional control loop based on the IBP control approach. To this end, the CBP controller proposed in Chapter 2 an IBP controller will be used in combination. Part of the modeling presented in Chapter 1 is used for the CBP control, an IBP control model is proposed. Then, ASTW algorithm is used making it possible to meet expectations.

In summary, the main contributions of this chapter are

- modeling of the both CBP control loop and the IBP control loop;
- design of ASTW controllers based on both CBP and IBP approaches;
- analysis of the obtained performances according to FAST/SIMULINK co-simulations.

4.2 System modeling

The main purposes of the controllers designed in this chapter are the limitation of the power at its rated value, the reduction of the platform pitch motion and the attenuation of the blade flap-wise root moment. The two first objectives can be achieved by the CBP control while the third one is fulfilled by IBP control. Since the CBP and IBP controllers can be separately designed as two independent control loops (see details in the sequel), two models are introduced in this section: the first one is the reduced CBP control loop model, whereas the second one is the reduced IBP control loop model which is acting on the behaviour of the blades.

4.2.1 Reduced CBP control model

The CBP model used in this section is the model detailed in Section 1.3.1, that is focused on the platform pitch motion and the rotor speed. Concerning the control objectives of CBP controller,

only 2 DOFs, the rotor rotation and the platform pitch, are considered. Recall here the nonlinear form of the 2 DOFs model (1.13); for a sake of clarity, rewrite (1.13) with new notations as following

$$\dot{x}_C \quad = \quad f_C(x_C, t) + g_C(x_C, t)u_C \tag{4.1}$$

with $x_C = [\varphi \ \dot{\varphi} \ \Omega_r]^T$, φ being the platform pitch angle, $\dot{\varphi}$ the platform pitch velocity and Ω_r the rotor speed, the control input being defined as $u_C = \beta_{col}$. This value is applied at each of the three blades.

4.2.2 Reduced IBP control model

The IBP model is focused on the blade behavior. It is obtained by the FAST linearization process and the MBC transformation algorithm (detailed in the sequel). The control objective of the IBP control loop is to reduce the blade fatigue loads; so, the dynamics of each blade is required. Thus, a 3 DOFs model, including the 1st flap-wise bending mode of each blade, is used for the IBP control loop and reads as

$$\dot{x}_I \quad = \quad A_I(\psi) \cdot x_I + B_I(\psi) \cdot u_I + B_{dI}(\psi) \cdot \delta_{dI} \tag{4.2}$$

with the state vector $x_I = [q^T \ \dot{q}^T]^T$ (q being the enabled DOFs) and the input vector u_I respectively defined as

$$x_I = \begin{bmatrix} q_1 \\ q_2 \\ q_3 \\ \dot{q_1} \\ \dot{q_2} \\ \dot{q_3} \end{bmatrix}, u_I = \begin{bmatrix} \tilde{\beta}_1 \\ \tilde{\beta}_2 \\ \tilde{\beta}_3 \end{bmatrix} \tag{4.3}$$

with q_i (resp. $\dot{q}_i$) ($1 \leq i \leq 3$) being the flap-wise bending deflection (resp. deflection rate) of blade $\#i$. δ_{dI} is the wind disturbance input. Recalling the blade coordinates system in Figure 1.4-left, the flap-wise bending deflection is the deflection along the x_{bi}-axis relative to the pitch axis (see Figure 4.1).

Note that system (4.2) is periodic with respect to rotor azimuth angle ψ; therefore, analysis and control design could be not straightforward. In order to avoid a periodic control design, the solution displayed in Chapter 1 is to average the periodic matrices over ψ. However, in this case, due to the fact that the DOFs (q_1, q_2, q_3 and their derivatives) are in the rotating frame of reference located in each blade respectively, the periodic information in the rotating frame is lost while averaging. Therefore, the multi-blade coordinate (MBC) transformation (G. Bir 2008), also known as *Coleman transformation*, is applied. Such coordinate transformation allows to transform the rotating frame into the non-rotating one. Then, the average process can be performed after the transformation; as a consequence, the periodic information on the blade can be kept.

Figure 4.1 – Blade#1 flap-wise bending deflection.

As shown in Figure 4.2, the rotating blade coordinates system on the left (detailed in Chapter 1) can be transferred by MBC into the fixed coordinates system on the right. This fixed one also known as rotor coordinates, expresses the cumulative behaviour of all of the rotor blades (G. S. Bir 2010). The x_{nr}-axis pointing to the shaft axis, the y_{nr}-axis is horizontal and perpendicular to the x_{nr}-axis and the z_{nr}-axis is vertical upward.

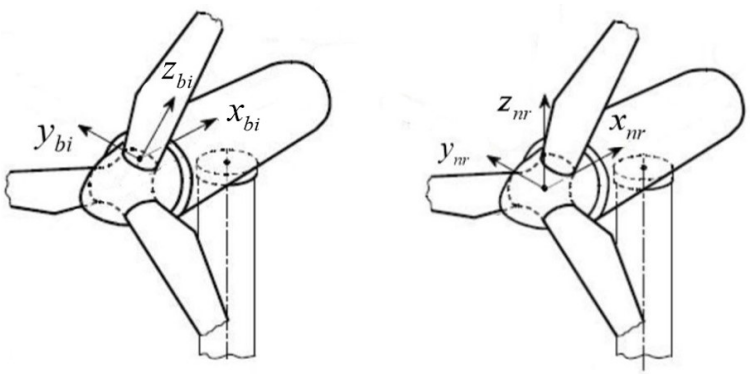

Figure 4.2 – Rotational blade root coordinates system (**left**) and fixed rotor coordinates system (**right**) ($i = \{1,\ 2,\ 3\}$ refers to the i^{th} blade) (Jelavić, Petrović, and Perić 2010).

Consider the following MBC transformation (G. Bir 2008)

$$\begin{aligned} q &= Tq_{nr} \\ u_I &= Tu_{nr} \end{aligned} \tag{4.4}$$

where the notation nr refers to the non-rotating frame; in the current case $q \in \mathbb{R}^3$, $q_{nr} \in \mathbb{R}^2$, $u_I \in \mathbb{R}^3$

and $u_{nr} \in \mathbb{R}^2$. T the transformation matrix reads as

$$T = \begin{bmatrix} cos(\psi) & sin(\psi) \\ cos(\psi + \frac{2\pi}{3}) & sin(\psi + \frac{2\pi}{3}) \\ cos(\psi + \frac{4\pi}{3}) & sin(\psi + \frac{4\pi}{3}) \end{bmatrix} \tag{4.5}$$

Remark 1. *The wind disturbance input vector is not in the rotating frame. Hence, δ_{dI} is not transformed by the MBC.* ■

According to (4.4), one has (G. Bir 2008)

$$\underbrace{\begin{bmatrix} q \\ \dot{q} \end{bmatrix}}_{x_I} = \begin{bmatrix} T & 0 \\ \Omega_r T_1 & T \end{bmatrix} \underbrace{\begin{bmatrix} q_{nr} \\ \dot{q}_{nr} \end{bmatrix}}_{x_{nr}} \tag{4.6}$$

with

$$T_1 = \begin{bmatrix} -sin(\psi) & cos(\psi) \\ -sin(\psi + \frac{2\pi}{3}) & cos(\psi + \frac{2\pi}{3}) \\ -sin(\psi + \frac{4\pi}{3}) & cos(\psi + \frac{4\pi}{3}) \end{bmatrix}. \tag{4.7}$$

Then, dynamics of x_I reads as

$$\underbrace{\begin{bmatrix} \dot{q} \\ \ddot{q} \end{bmatrix}}_{\dot{x}_I} = \begin{bmatrix} T & 0 \\ 0 & T \end{bmatrix} \underbrace{\begin{bmatrix} \dot{q}_{nr} \\ \ddot{q}_{nr} \end{bmatrix}}_{\dot{x}_{nr}} + \begin{bmatrix} \Omega_r T_1 & 0 \\ \Omega_r^2 T_2 + \dot{\Omega}_r T_1 & 2\Omega_r T_1 \end{bmatrix} \underbrace{\begin{bmatrix} q_{nr} \\ \dot{q}_{nr} \end{bmatrix}}_{x_{nr}} \tag{4.8}$$

with

$$T_2 = \begin{bmatrix} -cos(\psi) & -sin(\psi) \\ -cos(\psi + \frac{2\pi}{3}) & -sin(\psi + \frac{2\pi}{3}) \\ -cos(\psi + \frac{4\pi}{3}) & -sin(\psi + \frac{4\pi}{3}) \end{bmatrix} \tag{4.9}$$

Substituting (4.4), (4.6) and (4.8) into (4.2), the linearized model in the rotating frame is transformed into a non-rotating frame system. Then, one has (with $\dim(x_{nr}) = 4$)

$$\dot{x}_{nr} \;=\; A_{nr}(\psi) \cdot x_{nr} + B_{nr}(\psi) \cdot u_{nr} + B_{dnr}(\psi) \cdot \delta_{dI} \tag{4.10}$$

with the transformed matrices $A_{nr}(\psi)$, $B_{nr}(\psi)$ and $B_{dnr}(\psi)$ reading as

$$A_{nr}(\psi) = \begin{bmatrix} T^{-1} & 0 \\ 0 & T^{-1} \end{bmatrix} \left\{ A_I(\psi) \begin{bmatrix} T^{-1} & 0 \\ 0 & T^{-1} \end{bmatrix} - \begin{bmatrix} \Omega_r T_1 & 0 \\ \Omega_r^2 T_2 + \dot{\Omega}_r T_1 & 2\Omega_r T_1 \end{bmatrix} \right\} \tag{4.11}$$

$$B_{nr}(\psi) = \begin{bmatrix} T^{-1} & 0 \\ 0 & T^{-1} \end{bmatrix} B_I(\psi)T, \quad B_{dnr}(\psi) = \begin{bmatrix} T^{-1} & 0 \\ 0 & T^{-1} \end{bmatrix} B_d(\psi) \tag{4.12}$$

By applying the MBC transformation, the system (4.2) in the rotating frame is transformed into the non-rotating frame system (4.10). Therefore, the system metrics can be averaged after the MBC transformation without loss of the periodic information that depends on the rotor azimuth angle ψ. By this way, the controller can be designed in a straightforward way without considering the periodic dynamics. Then, the averaged state space model after MBC transformation reads as

$$\dot{x}_{NR} \quad = \quad A_{NR} \cdot x_{NR} + B_{NR} \cdot u_{NR} + B_{dNR} \cdot \delta_{dI} \tag{4.13}$$

with A_{NR}, B_{NR} and B_{dNR} the azimuth angle averaged state matrix, input matrix and wind input disturbance matrix respectively. For example, when the considered floating wind turbine is operating at a wind speed equal to $18m/s$ and rotor speed equal to its rated value $\Omega_{r0} = 12.1\ rpm$, one has

$$\begin{aligned} A_{NR} &= \begin{bmatrix} 0 & 0 & 1 & 0 \\ 0 & 0 & 0 & 1 \\ -18.7690 & -6.8117 & -5.3371 & -2.5478 \\ 6.8107 & -18.7620 & 2.5502 & -5.3487 \end{bmatrix}, \\ B_{NR} &= \begin{bmatrix} 0 & 0 \\ 0 & 0 \\ -636.8200 & -0.1149 \\ -0.1360 & -638.6200 \end{bmatrix}, B_{dNR} = \begin{bmatrix} 0 \\ 0 \\ -0.0671 \\ 0.17258 \end{bmatrix} \end{aligned} \tag{4.14}$$

As the modeling of Section 1.3.1, among a large operating domain, the model can be written as a class of nonlinear system

$$\dot{x}_{NR} \quad = \quad f_{NR}(x_{NR}, t) + g_{NR}(x_{NR}, t)u_{NR} \tag{4.15}$$

where

- $f_{NR}(x_{NR}, t)$ contains the term $A_{NR}(x_{NR}, t)$ and the term $B_{dNR}(x_{NR}, t) \cdot \delta_{dI}$, the uncertainties of the system and the perturbations introduced by wind, wave and other external environment;

- $g_{NR}(x_{NR}, t) = B_{NR}(x_{NR}, t)$ is the input function;

- $x_{NR} = [q_{tilt}\ q_{yaw}\ \dot{q}_{tilt}\ \dot{q}_{yaw}]^T$ with q_{tilt} and q_{yaw} the tilt (about the y_{nr}-axis) and yaw (about the z_{nr}-axis) components of blade flap-wise deflections respectively;

- β_{yaw} and β_{tilt} are the fictitious yaw and tilt component of blade pitch angles.

Note that the MBC transformation also allows to decouple the IBP control that is focused on load reduction, from the CBP control (Karl Stol et al. 2009). Furthermore, the control based on MBC transformation has almost same results as the periodic control (Karl Stol et al. 2009), but with reduced complexity.

4.3 Control problem statement

Recall that the control objectives in this chapter are to ensure the power output at rated meanwhile reducing the platform pitch motion and reducing the flap-wise load of blades. In the previous sections, both the first control objectives (power, platform pitch motion regulation) are achieved by collective blade pitch control. Here, the blade load (especially the blade flap-wise load) alleviation is also considered and can be ensured by separately adjusting the pitch angle of each blade, namely, by using the individual blade pitch control (E. A. Bossanyi 2003; Selvam et al. 2009; Van Engelen 2006).

The overall control scheme is shown in Figure 4.3. The IBP adjustment angles $\tilde{\beta}_1$, $\tilde{\beta}_2$ and $\tilde{\beta}_3$ are added to the CBP control input β_{col} but have a limited effect on the global behaviour of the power and platform pitch motion; in other words, there is a very reduced coupling between the CBP and IBP control (E. A. Bossanyi 2003; Jelavić, Petrović, and Perić 2010). Hence, these latter can be separately designed as two independent control loops while achieving their own control objectives.

4.3.1 Collective blade pitch control

The task of CBP control loop is to regulate power at rated P_0 meanwhile reducing the platform pitch motion. In this chapter, the generator torque is supposed to be fixed at its rated value Γ_{g0}, the objective being to focus the attention on the control of the hydrodynamic part of the wind turbine. As detailed in Section 2.2, define the desired rotor speed Ω_r^* as a function of platform pitch velocity

$$\Omega_r^* \quad = \quad \Omega_{r0} - k\dot{\varphi},\ k > 0 \tag{4.16}$$

Therefore, the controlled output associated to the system (4.1) is defined as

$$y_C \quad = \quad \Omega_r - \Omega_r^* \tag{4.17}$$

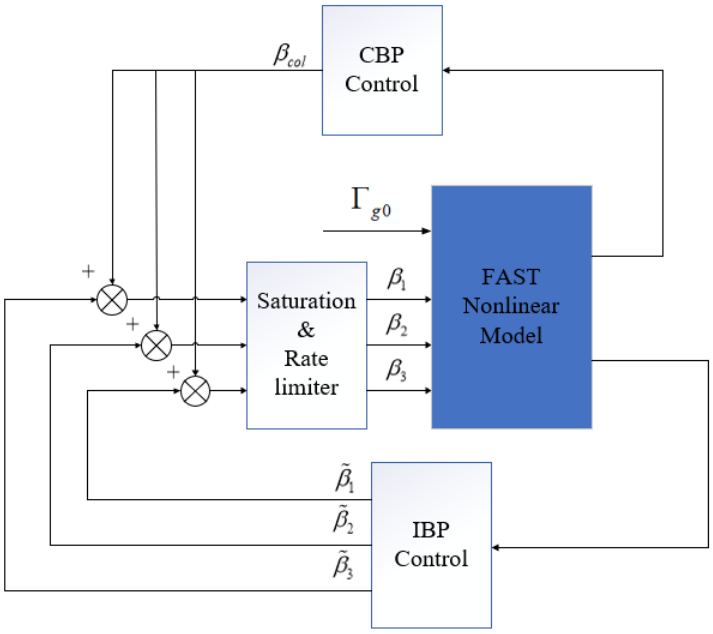

Figure 4.3 – Control scheme of the whole closed-loop system.

4.3.2 Individual blade pitch control

The rotor of wind turbine transforms the wind power into aerodynamic torque that drives the generator; at the same time, partial wind energy is transformed into thrust on the rotor that induces *load*. Due to the wind shear, tower shadow and turbulence, the wind speed and direction are varying across the rotor plane; these factors cause additional loads on the blades. These loads are related with the frequency of the rotor speed and can be decomposed along different modes, the main one being at the rotor speed frequency - this mode is denoted the *1p*-mode (*once-per-revolution*-see Figure 4.7). Other modes are existing at multiples of rotor speed and are denoted $2p$, $3p$ ... (E. A. Bossanyi 2003). The reduction of the $1p$-mode for each blade appears being a main objective of IBP control.

In this regard, the flap-wise bending moments (the moments about y_{bi}-axis see Figure 4.2) of each blade M_1, M_2 and M_3 are considered as the outputs of IBP control loop. Since the these moments are in the rotating blade coordinates system, MBC transformation is used. As detailed previously, the outputs M_1, M_2 and M_3 in the rotating frame can be transformed into the non-rotating frame. Then, one gets an output vector $y_{NR} = [M_{tilt}\ M_{yaw}]^T$, M_{tilt} (about the y_{nr}-axis see Figure 4.2) and M_{yaw} (about the z_{nr}-axis see Figure 4.2) respectively the tilt and yaw component of blade root flap-wise moment. As shown in (N. Wang, Wright, and Johnson 2016; Xiao, Yang, and Geng 2013),

among a large operating domain, this output can be written as

$$y_{NR} = h_{NR}(x_{NR}, t) + l_{NR}(x_{NR}, t)u_{NR}. \tag{4.18}$$

Remark 2. *Notice that the output y_{NR} depends on the control input vector u_{NR}; in this case, the relative degree of system* (4.15) *with output y_{NR} equals to 0.* ■

The main idea of IBP control is to force the magnitudes of M_{yaw} and M_{tilt} close to *zero* that reduces the blade flap-wise loads. MBC approach allows the decoupling between the IBP control that is responsible for load reduction, and the CBP control. Furthermore, it has been shown (E. A. Bossanyi 2003) that M_{yaw} and M_{tilt} can be treated independently by β_{yaw} and β_{tilt} respectively, *i.e.* it is possible to use two controllers for M_{yaw} and M_{tilt} alleviation, respectively.

Note that the following inverse MBC transformation should be applied after the controllers design in order to generate IBP control inputs $\tilde{\beta}_1$, $\tilde{\beta}_2$ and $\tilde{\beta}_3$ (see Figure 4.4)

$$\underbrace{\begin{bmatrix} \tilde{\beta}_1 \\ \tilde{\beta}_2 \\ \tilde{\beta}_3 \end{bmatrix}}_{u_I} = T \underbrace{\begin{bmatrix} \beta_{yaw} \\ \beta_{tilt} \end{bmatrix}}_{u_{NR}} \tag{4.19}$$

4.3.3 Overall control scheme

By a structural point-of-view, the overall control scheme is the combination of CBP and IBP control strategies (see Figure 4.3). Then, the overall control system design process can be summarized as follows

- design the CBP control for regulation of the power and reduction of the platform pitch motion;
- transform the three flap-wise blade flap-wise bending moments M_1, M_2 and M_3 into the fictitious ones M_{yaw} and M_{tilt}, design the control loop that provides β_{yaw} and β_{tilt} respectively, and obtain the components $\tilde{\beta}_1$, $\tilde{\beta}_2$ and $\tilde{\beta}_3$ thanks to the inverse MBC transformation;
- the *real* blade pitch angles β_1, β_2 and β_3, that are the "real" control inputs are equal to the sum of β_{col} with $\tilde{\beta}_1$, $\tilde{\beta}_2$ and $\tilde{\beta}_3$ respectively.

4.4 Control design

As detailed in the previous Section, the control scheme includes two control loops

- the first one is the CBP control loop focusing on the control of rotor speed and platform pitch motion;
- the second one is the IBP control loop producing an additional term to each blade pitch angle in order to reduce the variation of blade root flap-wise bending moments.

These two control loops can be independently designed (Jelavić, Petrović, and Perić 2010; E. A. Bossanyi 2003) as following.

CBP control loop

Recall that the relative degree of system (4.1) with y_C (4.17) is equal to 1. Therefore, according to Assumption 1, the sliding variable of CBP control can be defined as

$$S_1 = y_C \;=\; \Omega - \Omega^* \;=\; \Omega - (\Omega_r - k\dot{\varphi}) \tag{4.20}$$

IBP control loop

As recalled in Remark 2, the relative degree of system (4.15) with output y_{NR}, is equal to 0. Given that ASTW algorithm must be applied to systems with relative degree equal to 1, consider again the system (4.15)

$$\dot{x}_{NR} \;=\; f_{NR}(x_{NR}, t) + g_{NR}(x_{NR}, t)u_{NR}$$

with

$$y_{NR} \;=\; \begin{bmatrix} M_{tilt} \\ M_{yaw} \end{bmatrix} = h_{NR}(x_{NR}, t) + l_{NR}(x_{NR}, t)u_{NR}$$

A solution consists in defining a dynamic control law by increasing the relative degree of the system. Defining

$$\bar{x}_{NR} \;=\; u_{NR} \tag{4.21}$$

and $v_{NR} = \dot{u}_{NR}$ the *new* control input, system (4.15) can be reformulated as

$$\begin{aligned} \dot{x}_{NR} &= f_{NR}(x_{NR}, t) + g_{NR}(x_{NR}, t)\bar{x}_{NR} \\ \dot{\bar{x}}_{NR} &= v_{NR} \\ y_{NR} &= h_{NR}(x_{NR}, t) + l_{NR}(x_{NR}, t)\bar{x}_{NR} \end{aligned} \tag{4.22}$$

with $v_{NR} = [\dot{\beta}_{tilt}\ \dot{\beta}_{yaw}]^T$ the *new* control input.

Then, the relative degree of (4.22) with respect to $[\dot{\beta}_{tilt}\ \dot{\beta}_{yaw}]^T$ is equal to 1. Therefore, ASTW algorithm can be applied: the sliding variables of IBP loop are defined as $[S_2\ S_3]^T = [M_{tilt}\ M_{yaw}]^T$. Figure 4.4 depicts the IBP control scheme.

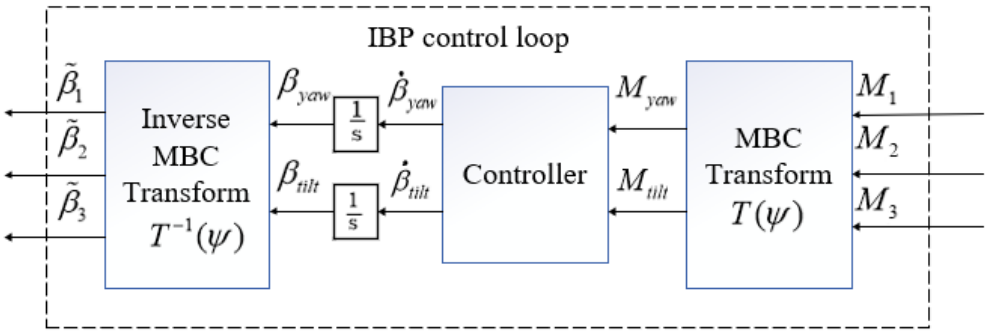

Figure 4.4 – Control scheme of IBP control loop.

Then, one has the sliding variable vector

$$S = \begin{bmatrix} S_1 \\ S_2 \\ S_3 \end{bmatrix} = \begin{bmatrix} \Omega - \Omega_r + k\dot{\varphi} \\ M_{tilt} \\ M_{yaw} \end{bmatrix} \tag{4.23}$$

and its dynamics reads as

$$\dot{S} \ = \ a(\cdot) + b(\cdot)v \tag{4.24}$$

with $a(\cdot)$ and $b(\cdot)$ unknown but bounded functions obtained from (4.1)-(4.22). The control input v is defined as

$$v \ = \ [\beta_{col}\ \dot{\beta}_{tilt}\ \dot{\beta}_{yaw}]^T \ = \ [v_1\ v_2\ v_3]^T \tag{4.25}$$

with

$$\begin{bmatrix} v_1 \\ v_2 \\ v_3 \end{bmatrix} = \begin{bmatrix} -k_{11}|S_1|^{\frac{1}{2}}\text{sign}(S_1) - \int_0^t k_{12}\text{sign}(S_1)d\tau \\ -k_{21}|S_2|^{\frac{1}{2}}\text{sign}(S_2) - \int_0^t k_{22}\text{sign}(S_2)d\tau \\ -k_{31}|S_3|^{\frac{1}{2}}\text{sign}(S_3) - \int_0^t k_{32}\text{sign}(S_3)d\tau \end{bmatrix} \tag{4.26}$$

The gains k_{i1} and k_{i2} ($i = \{1,\ 2,\ 3\}$) are evolving according to adaptation law (2.21) [1].

1. Notice that the main objective of this chapter is to verify that an adaptive super-twisting approach is efficient for the IBP control of FWT. In order to clearly analyze the results of adaptive controller, only the traditional ASTW controller is used.

4.5 Simulations and analysis

As previously, the nonlinear OC3-Hywind 5MW floating wind turbine model from NREL is simulated in this section; such nonlinear model is built in FAST software and is regarded as a benchmark in many of wind turbines studies. Recall that the parameters of this wind turbine are shown in the Table 1.1. In addition, the control is developed in the SIMULINK environment and linked with the FAST model by an s-function. Finally, the co-simulations between FAST and SIMULINK are made on the full DOFs FAST nonlinear model while the control is designed based on the reduced DOFs model as detailed previously. Three controllers are used in the following simulations

- **GSPI-CBP**: the baseline GSPI controller with collective blade pitch control (J. Jonkman 2008b);

- **ASTW-CBP**: the adaptive super-twisting controller with collective blade pitch control; only υ_1 is used of (4.26) (see Chapter 2) given that there is a single control input β_{col};

- **ASTW-CIBP**: The adaptive super-twisting controller that combines collective blade pitch control and individual blade pitch control (4.26). The controller parameters used for this controller being shown in Table 4.1 and the parameter k of sliding variable S_1 in (4.23) is equal to 16.7.

Table 4.1 – ASTW-CIBP controller parameters

Gains	Parameters
k_{11}, k_{12}	$k_{1m} = 10^{-4}$, $\epsilon = 0.03$, $\omega = 1$, $\chi = 0.001$, $\mu = 0.05$, $k = 10^{-4}$
k_{21}, k_{22}	$k_{1m} = 10^{-6}$, $\epsilon = 0.05$, $\omega = 1$, $\chi = 0.003$, $\mu = 0.4$, $k = 0.01$
k_{31}, k_{32}	$k_{1m} = 10^{-6}$, $\epsilon = 0.05$, $\omega = 1$, $\chi = 0.003$, $\mu = 0.2$, $k = 0.01$

The use of these controllers has several objectives: comparison between standard (GSPI) and advanced controllers (ASTW), and comparison between CBP and CBP/IBP control structures. In addition, two cases of wind and wave conditions are simulated in the sequel

- **Scenario 1**. 18 m/s constant wind with still water (*i.e.* no wave);

- **Scenario 2**. 18 m/s stochastic wind with 15% turbulence intensity; irregular wave with significant height of 3.25 m and peak spectral period of 9.7 s (see Figure 3.2).

Note that the wind speed of both scenarios is in above rated region, and all the simulations are

made in 600 seconds and Euler integration with sample time fixed at 0.0125 seconds. Moreover, since there is no blade pitch actuator in the FAST nonlinear model, and in order to be as close as possible from the real system, the blade pitch angle is saturated between [0°, 90°] and the maximum blade pitch rated is limited at $8°/s$ (see Table 1.1).

4.5.1 Scenario 1. Constant wind and still water condition

In this scenario, ASTW-CBP and ASTW-CIBP control strategies are compared, the objective being to check the interest to include a IBP control loop. Firstly, Figure 4.5 displays that both the CBP and CIBP controllers ensure the rotor speed around its rated value 12.1 rpm and limited the platform pitch motion (*i.e.* reduced the platform pitch angle variation). Furthermore, Figure 4.6 shows that the tilt and yaw moment are forced around zero thanks to the CIBP controller; as a consequence, the blade root flap-wise moment are strongly reduced compared to the CBP controller (see Figure 4.6-right).

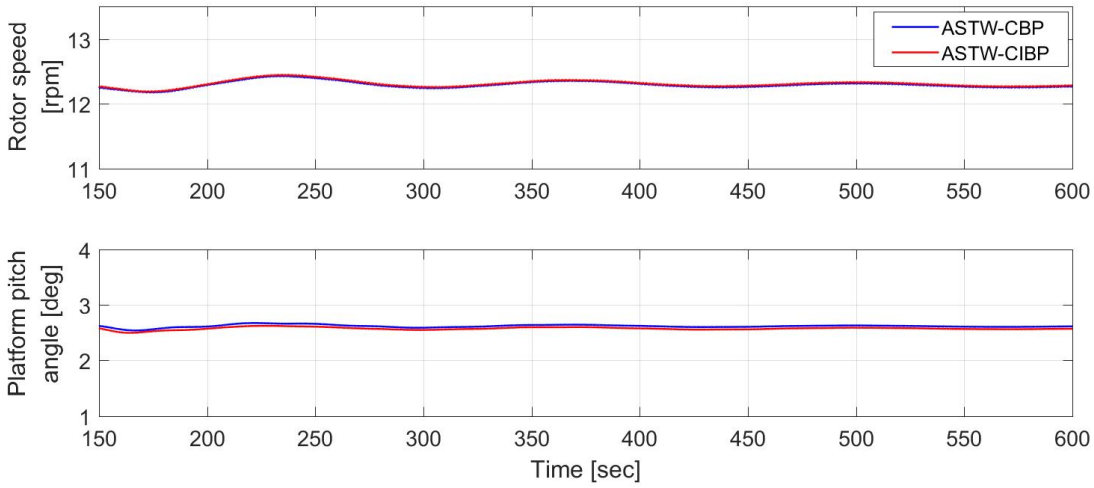

Figure 4.5 – **Scenario 1.** Rotor speed Ω_r and platform pitch angle φ versus time (sec).

Specifically, from the power spectral density (PSD) of blade #1 root flap-wise moment displayed by Figure 4.7, one can find that the load reduction of CIBP control is strongly acting on the $1p$ component of the blade load. Meantime, the rotor speed and platform pitch motion are not affected as shown in Figure 4.5 (the trajectories of CBP and CIBP control are highly coincidence): as mentioned in previous section, the collective pitch control and the individual pitch control are decoupled. Figure 4.8 shows the blade #1 pitch angle obtained with the two controllers. It is clear that CIBP controller is acting much more on the blade pitch angles.

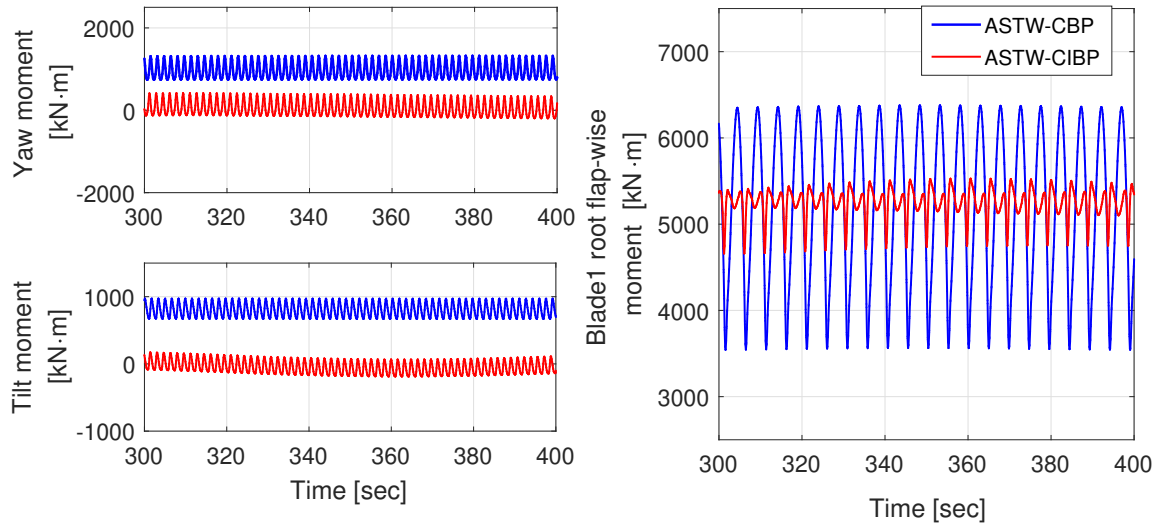

Figure 4.6 – **Scenario 1.** Transformed yaw moment M_{yaw} (**left-top**), tilt moment M_{tilt} (**left-bottom**) and blade #1 root flap-wise moment (**right**) versus time (*sec*).

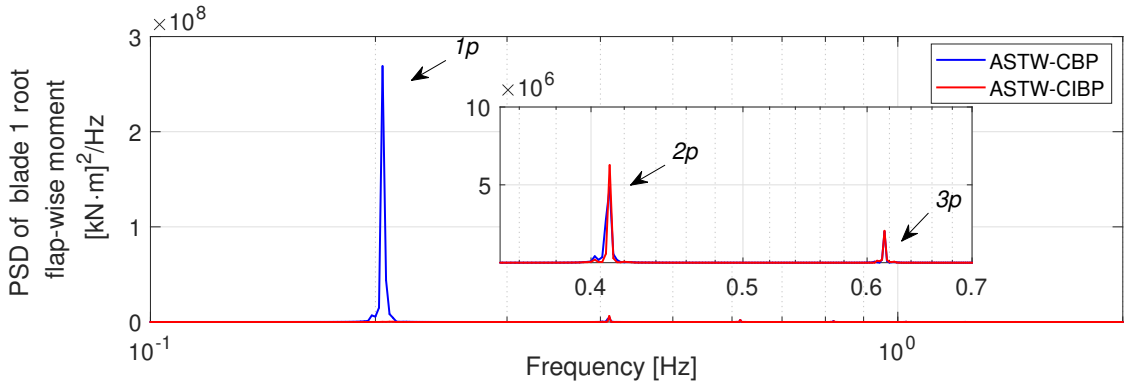

Figure 4.7 – **Scenario 1.** Power spectral density of blade #1 root flap-wise moment.

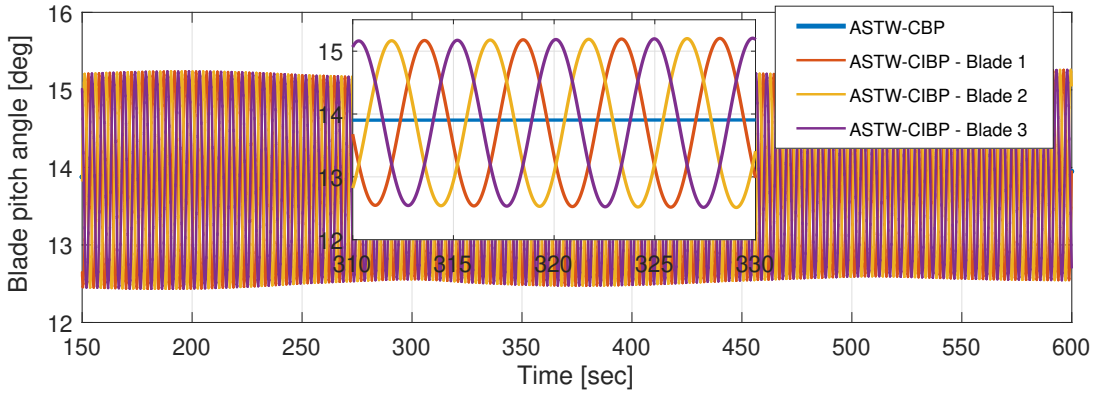

Figure 4.8 – **Scenario 1.** Blade pitch angles versus time (*sec*).

4.5.2 Scenario 2. Stochastic wind and irregular wave condition

Previous scenario shows that both the ASTW controllers allow to achieve all the control objectives in ideal conditions and shows the interest to introduce an IBP control loop. In Scenario 2, a more realistic situation is considered with the 3 following controllers: GSPI-CBP, ASTW-CBP and ASTW-CIBP. By a similar way as previous chapters, the performances of the 3 controllers are compered by using the indices as follows:

- root mean square (RMS) of rotor speed error, power error, platform rotations (roll, yaw and pitch), and platform pitch rate;
- variation (VAR) of the blade pitch angle that is an image of the pitch actuator use;
- damage equivalent load (DEL) of the tower base fore-aft, side-to-side and torsional moments, DEL of averaged blade root flap-wise and edge-wise bending moments of the three blades, and DEL of mooring lines.

As previously, all of these performance indicators are normalized with respect to GSPI-CBP controller (see the red line in Figures 4.9 and 4.10 that represents the normalized values for GSPI-CBP controller). If the value of a normalized indicator is smaller than 1, it means that the performance is better than GSPI-CBP; on the contrary, if the value of a normalized indicator is larger than 1, it means that the performance is worse than GSPI-CBP.

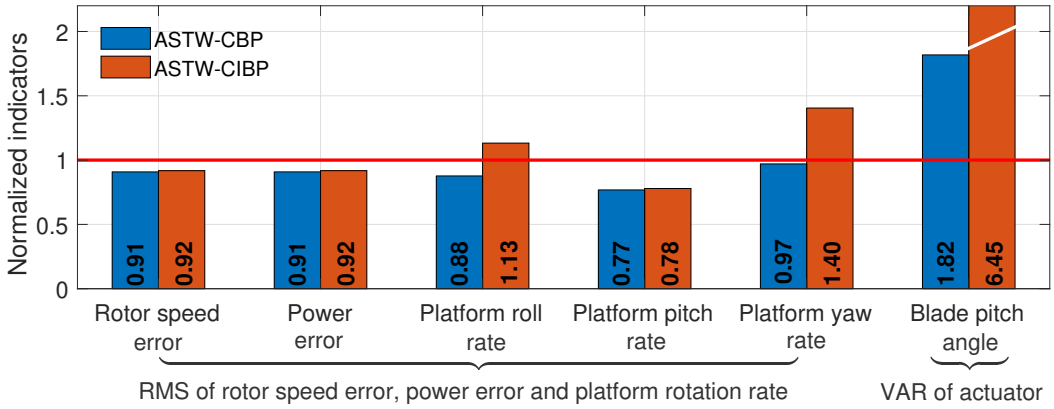

Figure 4.9 – **Scenario 2.** Normalized RMS and VAR values of the 3 controllers.

Figure 4.9 shows that, for two of the main control objectives (rotor speed/ power regulation and platform pitch motion reduction), ASTW-CBP and ASTW-CIBP controllers have similar perfor-

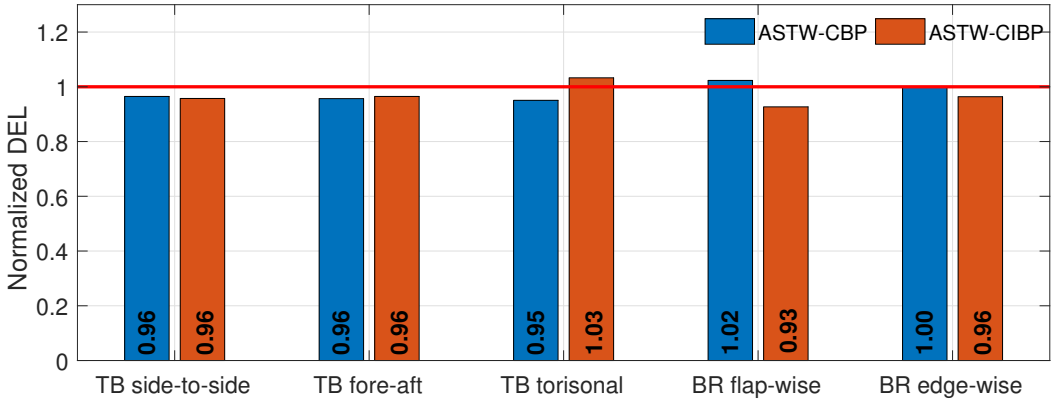

Figure 4.10 – **Scenario 2.** Normalized tower base (TB) and blade root (BR) DEL of the 3 controllers.

mances allowing reduction of rotor speed error (by 8-9%) and platform pitch rate (by 22-23%), versus GSPI-CBP. As previously mentioned, there is no coupling between CBP and IBP control loops; hence, ASTW-CBP and ASTW-CIBP have similar performances on rotor speed and platform pitch rate. As shown by Figure 4.11, the time series of ASTW-CBP and ASTW-CIBP in terms of rotor speed (power) and platform pitch angle are almost identical.

Furthermore, ASTW-CBP controller has also reduced the platform roll and yaw rates; on the contrary, ASTW-CIBP controller induces more important platform roll and yaw rates due to a greatly increased blade pitch actuation (H. Namik and K. Stol 2014). However, given that the magnitudes of platform roll and yaw are relatively small (see Figure 4.11), they have a very limited influence on the stability of the whole system.

Figure 4.10 shows the DEL results: it is clear that ASTW-CBP control law reduces the platform base loads but increases the blade root flap-wise load. For the ASTW-CIBP, the tower base side-to-side and fore-aft loads have similar reductions than ASTW-CBP, while the torsional load increases by 3%. Nonetheless, Figure 4.11 shows that the torsional load is very reduced comparing to the side-to-side and fore-aft loads of tower base: then, an increasing of 3% is meaningless for the load of tower. Furthermore, ASTW-CIBP reduces the blade root flap-wise load ($1p$ load - see Figure 4.12).

Generally, ASTW-CIBP control strategy has not only better performances on the rotor speed (power) regulation and platform pitch motion reduction than GSPI-CBP as ASTW-CBP, but also can reduce the fatigue load of blades, all of which being crucial problems of the floating wind turbine control. Moreover, this controller requires very few knowledge of system model and the controller

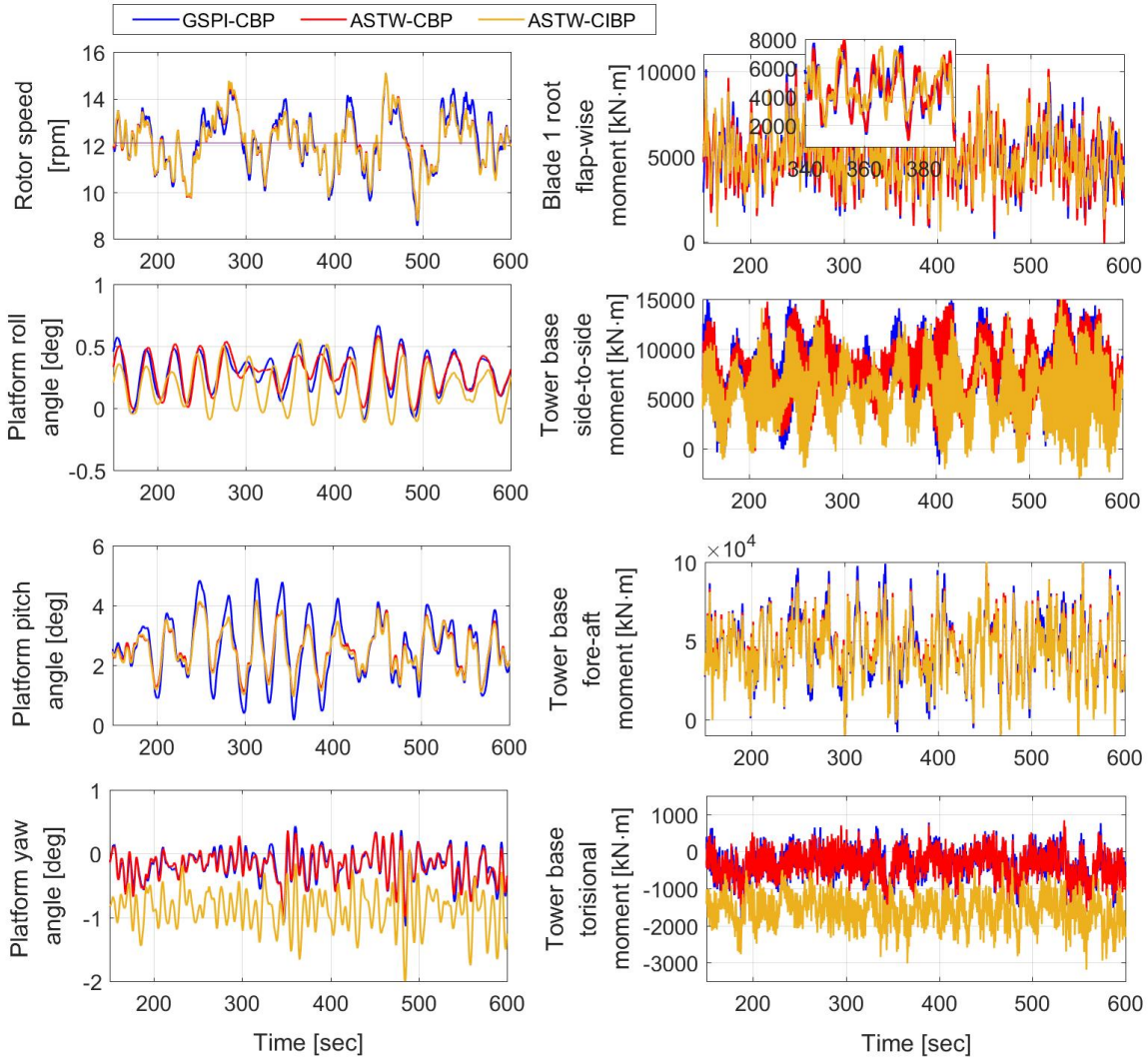

Figure 4.11 – **Scenario 2.** System variables of versus time (*sec*).

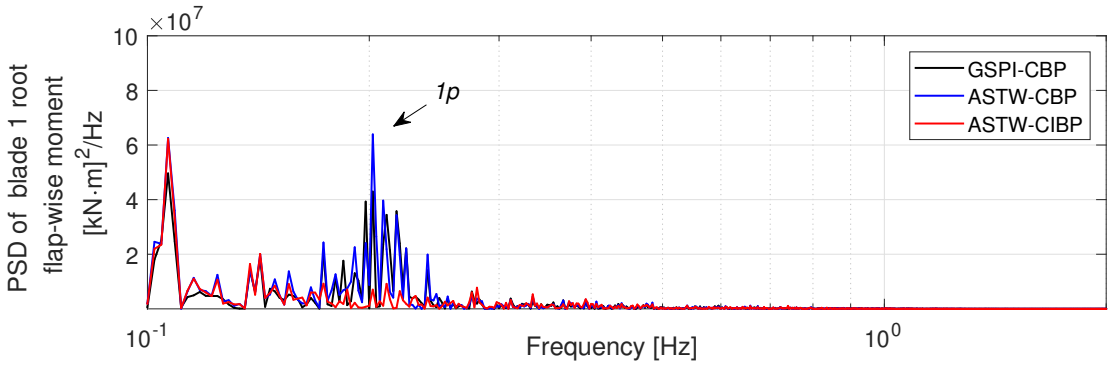

Figure 4.12 – **Scenario 2.** PSD of blade #1 root flap-wise moment.

gains can be dynamically adapted with the uncertainties and perturbations (see Figure 4.13) that largely reduces the parameters tuning effort.

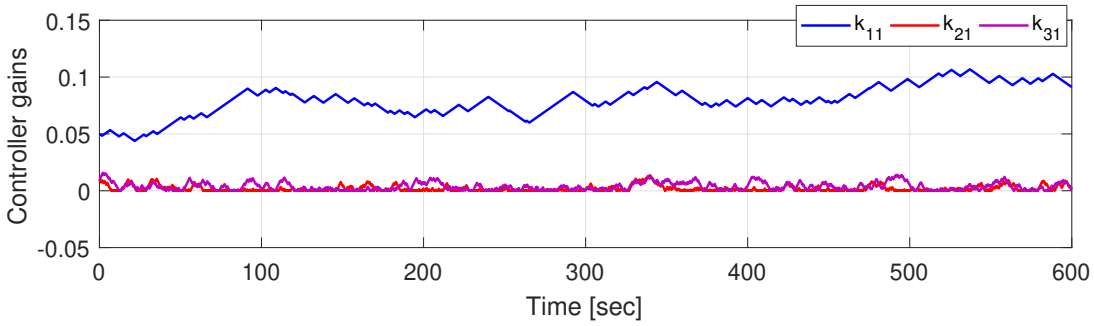

Figure 4.13 – **Scenario 2.** Controller gains of ASTW-CIBP algorithm (4.26) versus time (*sec*).

However, such improvement has a cost that is a more aggressive actuator use, as shown by Figures 4.9 (VAR of actuator) and 4.14: the variation of ASTW-CBP increases by 82% versus CBP-GSPI whereas it is worst with ASTW-CIBP controller. Notice that, given that the dynamics of blade pitch actuators is taken into account in the simulations, such intensive use of theses actuators is practically acceptable.

4.6 Conclusions

Super-twisting algorithms with gain adaptation laws, based on collective/individual blade pitch approach, have been applied to the floating wind turbines control problem in Region III. Such control algorithms strongly reduce the workload of parameters tuning: only few knowledge of system model is required that makes such control strategies well-adapted to the floating wind turbine systems.

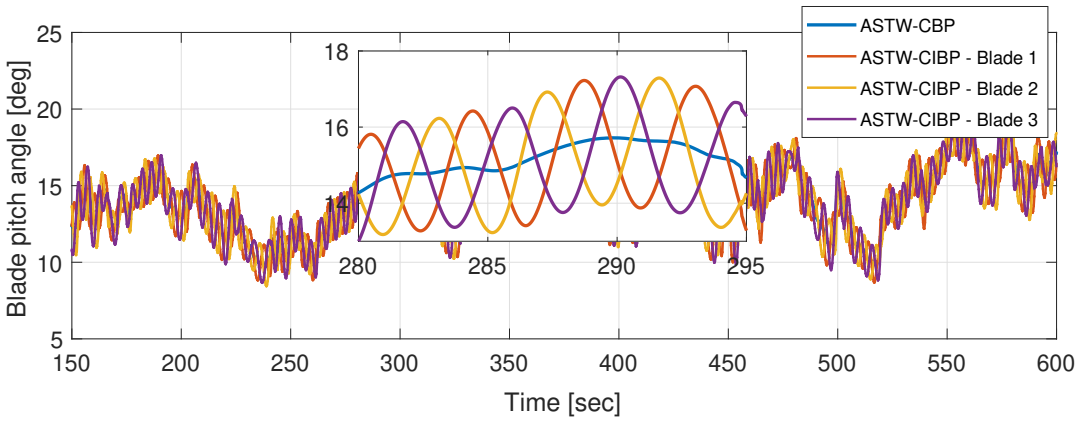

Figure 4.14 – **Scenario 2.** Blade pitch angle of ASTW-CBP and ASTW-CIBP versus time (*sec*).

The control goals are the regulation of the rotor speed, the reduction of the platform pitch motion and the reduction of the fatigue load of the blades. The simulations made on FAST software show that the collective control loop and individual blade pitch control loop are well decoupled by the MBC transformation. Then, the CIBP based ASTW algorithm gives not only better performances on the power regulation and platform pitch motion reduction than CBP controllers, but also provides better performances on the blade load reduction.